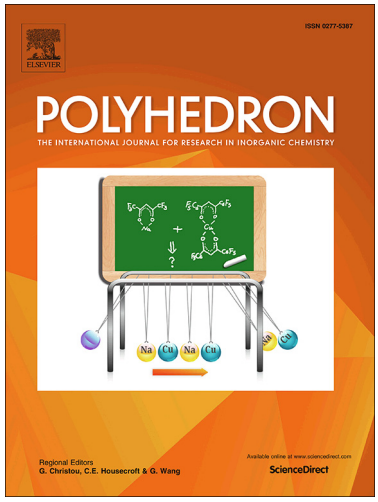

Accessing Decavanadate Chemistry With Tris(HYDROXYMETHYL)Aminomethane, And Evaluation Of Methylene Blue Bleaching

Juliana M. Missina, Luiza B.P. Leme, Kahoana Postal, Francielli S. Santana, David L. Hughes, Eduardo L. de Sá, Ronny R. Ribeiro, Giovana G. Nunes

PII: S0277-5387(20)30071-1
DOI: https://doi.org/10.1016/j.poly.2020.114414
Reference: POLY 114414

To appear in: *Polyhedron*

Received Date: 22 November 2019
Revised Date: 24 January 2020
Accepted Date: 27 January 2020

Please cite this article as: J.M. Missina, L.B.P. Leme, K. Postal, F.S. Santana, D.L. Hughes, E.L. de Sá, R.R. Ribeiro, G.G. Nunes, Accessing Decavanadate Chemistry With Tris(HYDROXYMETHYL)Aminomethane, And Evaluation Of Methylene Blue Bleaching, *Polyhedron* (2020), doi: https://doi.org/10.1016/j.poly.2020.114414

ACCESSING DECAVANADATE CHEMISTRY WITH TRIS(HYDROXYMETHYL)AMINOMETHANE, AND EVALUATION OF METHYLENE BLUE BLEACHING

Juliana M. Missina[1*], Luiza B. P. Leme[1], Kahoana Postal[1], Francielli S. Santana[1], David L. Hughes[2], Eduardo L. de Sá[1], Ronny R. Ribeiro[1], and Giovana G. Nunes[1]

[1]*Departamento de Química, Universidade Federal do Paraná, Curitiba-PR, Brazil*

[2]*School of Chemistry, University of East Anglia, Norwich NR4 7TJ, UK*

Graphical abstract

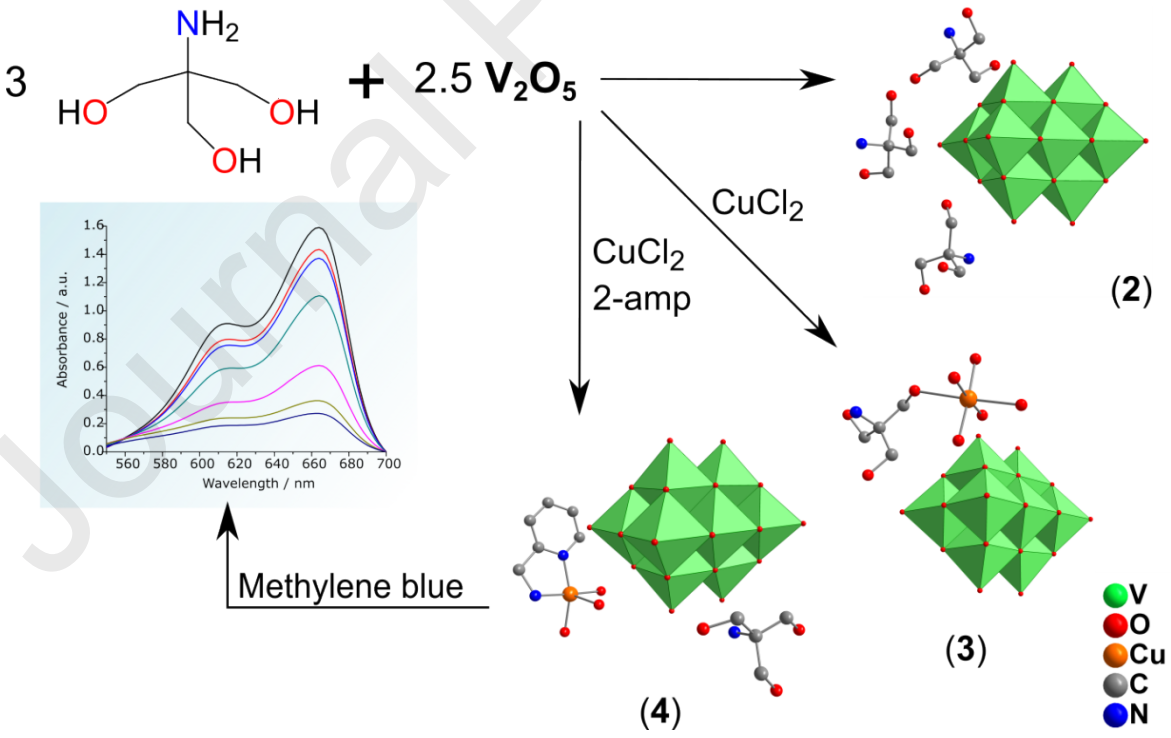

Abstract

Two decavanadates $(trisH)_4[H_2V_{10}O_{28}]\cdot 10H_2O$ (**1**) and $(trisH)_6[V_{10}O_{28}]$ (**2**) have been synthesised from $NaVO_3$ or V_2O_5 in an aqueous solution of tris(hydroxymethyl)aminomethane (tris). Bimetallic derivatives $[Cu(OH_2)_5(trisH)]_2[V_{10}O_{28}]\cdot 6H_2O$ (**3**) and $[Cu(OH_2)_3(2–amp)]_2(trisH)_2[V_{10}O_{28}]\cdot 2H_2O$ (**4**) were obtained by the addition of $CuCl_2$ or $CuCl_2$ / 2–amp (2–(aminomethyl)pyridine) to the route that gave **2**. The products were characterised by single-crystal X-ray diffractometry, thermogravimetric analysis, FTIR, Raman and EPR spectroscopies. Moreover, **4** was effective in bleaching a methylene blue (MB) solution under natural light in acidic media by either degradation of the dye or precipitation of a MB-decavanadate salt depending on the experimental conditions.

Keywords: decavanadate; copper(II); tris(hydroxymethyl)aminomethane; 2–(aminomethyl)pyridine; methylene blue

1. INTRODUCTION

Polyoxovanadates (POV) form a subclass of metal oxoanions that has attracted considerable attention due to its rich structural diversity [1, 2], electronic properties [3, 4], and applications in biology [5, 6], material sciences [7, 8], magnetism [9, 10], and catalysis [11-13]. Decavanadate, $[H_xV_{10}O_{28}]^{(6-x)-}$ (V_{10}), is the most stable vanadium(V) species in acidic conditions [14] and has been

widely investigated in its interaction with several biomolecules, interfering in a number of biological processes. The anion has also been explored in the crystallisation of proteins [15] and in the design of supramolecular assemblies with 1D, 2D and 3D networks built via electrostatic forces and intermolecular interactions, such as hydrogen bonding, $\pi-\pi$ stacking, etc [16, 17].

Decavanadate has been associated with organic cations [16] or cation complexes of other transition metals, including Mn^{II} [18], Zn^{II} [19], Co^{II} [19], Ni^{II} [20], $Cu^{I/II}$ [21] and Ag^{I} [19]. Structures with a second metal ion produced V_{10}–scaffolds decorated with metal complexes through their terminal or bridging oxygen atoms [18, 19], heterometallic polymers [22, 23], or ionic salts in which the two metals are separated [24, 25]. The combination of V_{10} with Cu^{II} complexes has yielded structures that fall into all these classes [21-26]. These compounds have been explored in the selective adsorption of CO_2 over N_2, and as catalysts of cycloaddition reactions and oxidation of adamantane [21].

Polyoxovanadates containing tris(hydroxymethyl) derivatives are well known [27]. The most common structures include trisalkoxo-derived hexavanadates [28-35], whereas functionalised V_4 [33, 36], V_7 [33] and V_{10} [37] structures were seldom described. Among them, tris(hydroxymethyl)aminomethane has been especially used for additional functionalisation with a variety of organic groups [31, 38, 39]. Nevertheless, polyoxovanadates having protonated tris(hydroxymethyl)aminomethane as a counterion remain rare. To the best of our knowledge, two structures have been crystallographically characterised: a mixed-valence hexadecavanadate prepared under hydrothermal conditions [40], and a

decavanadate anion decorated with manganese aquo complexes [18], the latter previously reported by our group following another methodology.

Recently, the interest in the rationalisation of synthetic routes that produce V_{10}–based hybrid compounds has quickly increased, and alternative methodologies at room temperature have already arisen [41]. Among the possible starting materials, vanadium pentoxide (V_2O_5) is a convenient reactant since it does not provide extra metal ions. Even though some efforts have been made to overcome its poor solubility in water and to avoid the use of strong bases or hydrogen peroxide, the improvement of yields and the elimination of impurities generated by precipitation products remain as common challenges [42, 43].

Methylene blue (MB) is a hazardous cationic dye widely employed in the textile industry and frequently discharged directly in natural water bodies such as rivers and lakes [44]. Metal oxides doped with vanadium and several polyanionic clusters, including polyoxometalates, have been applied for removing MB from aqueous solution by catalytic degradation, flocculation or adsorption [45-47]. The degradation properties of organic dyes by POV is well known; however, only very recently, this class of compounds started to be evaluated in its potential to MB bleaching. The few reports showed both rapid MB adsorption and excellent photocatalytic degradation of the dye depending on the nature of the POV and the reaction conditions [45, 48, 49].

We describe herein the development of a facile methodology to obtain decavanadate salts in an aqueous solution of the common buffer

tris(hydroxymethyl)aminomethane (tris) at room temperature. The high purity and yield of $(trisH)_6[V_{10}O_{28}]$ (**2**) allowed us to expand the route to produce two new V_{10}-copper(II) products by adding $CuCl_2$ and 2–(aminomethyl)pyridine (amp) to the reaction medium. Moreover, the product $[Cu(OH_2)_3(2–amp)]_2(trisH)_2[V_{10}O_{28}]\cdot 2H_2O$ (**4**) showed efficient bleaching of a MB aqueous solution.

2. EXPERIMENTAL

2.1. Materials and methods

2.1.1. General considerations

Ultrapure water (Milli-Q, Millipore type 1, resistivity of 18.2 MΩ cm at 25 °C) was employed to prepare all solutions used in the syntheses and reactions with MB. Reactants vanadium pentoxide (V_2O_5, ≥ 99.6%), sodium metavanadate ($NaVO_3$, 98.0%), methylene blue (97%), 2–amino–2–hydroxymethyl–propane–1,3–diol (tris, 99.0%), 2–(aminomethyl)pyridine (2–amp, 98.0%) and copper(II) chloride ($CuCl_2$) were purchased from Sigma-Aldrich and used with no further purification. Hydrogen peroxide (H_2O_2) 35% was acquired from Neon.

2.1.2. Analytical methods and instruments

Vanadium and copper contents were obtained by inductively coupled plasma optical emission spectrometry (ICP-OES) from a Perkin Elmer Optima 8300 series spectrometer. Microanalyses were carried out in a Perkin Elmer 2400 Series Elemental Analyzer. FTIR spectra were registered from KBr pellets on a Bomen MB100 spectrophotometer, from 400 to 4000 cm^{-1}. Raman spectra were obtained with a Raman Confocal Witec alpha 300R microscope, which focuses the incident radiation on a 1-μm^2 area. Spectra were recorded using He-Ne (633.120 nm) laser excitation over the range of 0 to 2750 cm^{-1}. Electron paramagnetic resonance (EPR) data were recorded with an X-band (9.5 GHz) Bruker EMX-Micro spectrometer from the pulverised solid at 77 and 298 K. Spectra simulations were run with the EasySpin software [50]. ^{51}V NMR spectra were acquired at 295 K in H_2O/D_2O (10%) in a Bruker Avance 400 MHz spectrometer using $VOCl_3$ (neat, capillary) as reference for ^{51}V. Electronic spectra were recorded in a PerkinElmer Lambda 1050 UV−vis spectrophotometer in the spectral range of 550–700 nm using a 1 cm quartz cuvette. Thermogravimetric analyses (TGA) were performed on a Netzsch STA449 F3 Jupiter analyser instrument with a silicon carbide furnace. Aluminum pans were used for heating samples (approximately 4 mg) from 25 °C to 900 °C at a heating rate of 10 °C min^{-1} using N_2/O_2 as carrier gas.

2.1.3. Syntheses

Preparation of $(trisH)_4[H_2V_{10}O_{28}]\cdot 10H_2O$ (**1**)

A suspension of $NaVO_3$ (0.610 g, 5.00 mmol) in 20 mL of water at 100 °C was stirred until complete dissolution. The resulting solution was left to cool down to

room temperature, when the pH was adjusted to 4.0 with HCl 1.0 mol L^{-1} and the addition was made of an aqueous solution of tris (0.360 g, 3.00 mmol, in 10 mL). After stirring for 1 h, the resulting orange solution received an ethanol overlayer and was stored at 4 °C. Orange crystals, formed after 3 days, were washed with cold ultrapure water and dried in air (0.480 g, 0.300 mmol). Product **1** was soluble in water and dimethylsulfoxide. FTIR (KBr, cm^{-1}, s = strong, m = medium, w = weak, br = broad): 3448(br), 1630(s), 1490(m), 1400(m), 1072(m), 955(s), 839(s), 741(m), 604(m).

Preparation of $(trisH)_6[V_{10}O_{28}]$ (**2**)

A 40 mL aqueous suspension of V_2O_5 (0.460 g, 2.50 mmol) received 10 mL of an aqueous solution of tris (0.360 g, 3.00 mmol). After stirring at room temperature for 2 days, the initial suspension turned into an orange solution that was then stored at 4 °C with an overlayer of isopropanol. Orange crystals formed after 2 weeks were dried in air (0.540 g, 0.320 mmol). Yield: *ca* 63% based on vanadium. Product **2** was soluble in water and dimethylsulfoxide. Elemental analysis: calculated (%) for $C_{24}H_{72}N_6O_{46}V_{10}$ (**2**): V, 30.1; C, 17.2; H, 4.30; N, 5.00; found (%) for **2**: V, 30.9; C, 17.0; H, 4.20; N, 4.90. FTIR (KBr, cm^{-1}): 3392(br), 3126(br), 1593(s), 1498(w), 1269(w), 1059(m), 955(s), 841(m), 737(m), 600(m), 449(m).

Preparation of $[Cu(OH_2)_5(trisH)]_2[V_{10}O_{28}]\cdot 6H_2O$ (**3**)

V_2O_5 (0.460 g, 2.500 mmol) was suspended in 40 mL of water and 10 mL of an aqueous solution of tris (0.360 g, 3.00 mmol) were added under stirring at room temperature. To the orange solution obtained after 48 h, 5 mL of an aqueous solution of $CuCl_2\cdot 2H_2O$ (0.170 g, 1.00 mmol) were added. After stirring for 14 h,

the precipitate formed was filtered off, and the liquor mother received an overlayer of isopropanol. Orange crystals were isolated after 20 days under storage at 4 °C (0.520 g, 0.320 mmol). Yield: *ca* 64% based on vanadium. Product **3** was soluble in water. Elemental analysis: calculated (%) for $C_8H_{56}N_2O_{50}V_{10}Cu_2$ (**3**): V, 31.5; Cu, 7.90; C, 5.94; H, 3.49; N, 1.73. found (%) for **3**: V, 31.4; Cu, 7.80; C, 6.20; H, 3.51; N, 1.75. FTIR (KBr, cm^{-1}): 3070(br), 1583(m), 1485(w), 1294(w), 1054(m), 941(s), 839(m), 744(m), 590(m), 455(m).

Preparation of $[Cu(OH_2)_3(2–amp)]_2(trisH)_2[V_{10}O_{28}]\cdot 2H_2O$ (**4**)

Product **4** was synthesised through a methodology analogous to that used for obtaining product **3**, except for the addition of 2–amp (103.5 μL, 1.00 mmol) to the orange solution along with the 5 mL of aqueous $CuCl_2\cdot 2H_2O$ (0.170 g, 1.00 mmol). After stirring for 48 h the green precipitate was filtered off and received an overlayer of isopropanol. Dark green crystals were isolated after 12 days under storage at 4 °C (0.280 g, 0.160 mmol). Yield: *ca* 33% based on vanadium. Elemental analysis: calculated (%) for $C_{20}H_{56}N_6O_{42}V_{10}Cu_2$ (**4**): V, 30.16; Cu, 7.52; C, 14.22; H, 3.34; N, 4.98; found (%) for **4**: V, 30.2; Cu, 7.42; C, 14.3; H, 3.36; N, 4.88. FTIR (KBr, cm^{-1}): 3495(br), 3236(br), 3088(br), 1581(m), 1481(w), 1284(w), 1153(w), 1063(m), 941(s), 835(m), 736(m), 578(m).

Direct reaction of decavanadate with methylene blue in solution

A suspension of $NaVO_3$ (0.609 g, 5.00 mmol) in 30 mL of water was heated under stirring until complete dissolution. The pH of the resulting colourless solution was adjusted to 4.0 giving an orange solution typical of the decavanadate. An

aqueous solution of MB (0.096 g, 0.3 mmol) was slowly diffused for a period of 24 h at room temperature. The green crystals formed were filtered, washed 5 times with 2.0 mL of water and dried in air (0.203 g, 0.086 mmol). Yield: *ca* 17% based on V. **MBV_{10}** was slightly soluble in water, dmso, methanol and ethanol. Elemental analysis: calculated (%) for $C_{64}H_{104}N_{12}S_4O_{43}V_{10}$ (**MBV_{10}**): V, 21.5; C, 32.5; H, 4.43; N, 7.10; found (%) for **MBV_{10}**: V, 23.8; C, 32.6; H, 3.92; N, 7.03. FTIR (KBr, cm^{-1}): 3431(br), 3348(br), 1599(s), 1489(m), 1441(w), 1392(s), 1356(s), 1252(m), 1221(m), 1178(m), 1153(m), 1040(w), 964(s), 887(s), 831(s), 760(w), 669(w), 607(w), 538(w), 451(w).

2.2. Single-crystal X-ray diffraction analysis

Crystals of **1**–**4** were mounted on a Bruker D8 Venture diffractometer with a Photon 100 CMOS detector. For samples **1**, **2** and **4** the Mo-Kα radiation and a graphite monochromator were used; for sample **3**, a Cu-Kα μS-microsource radiation and Gobbel mirrors monochromator were chosen. Intensity data were measured by thin-slice ω- and φ-scans. Data processing employed the APEX2 program [51] for sample **1** and the APEX3 program [52] for the other samples. The structures were determined by the intrinsic phasing routines in the SHELXT [53] program and refined by full-matrix least-squares methods, on F^2's, in SHELXL [53]. Refinement of non-hydrogen atoms was carried out using anisotropic thermal parameters. Scattering factors for neutral atoms were taken from the literature [54]. Computer programs used in the analysis were run through WinGX [55], and figures that refer to the structures were made using programs

ORTEP3 [55] and Diamond 4 [56]. Refinement details for each of the products can be found in the Supplementary Material.

2.3. Bleaching of methylene blue in aqueous solution

In a typical procedure, 6.0×10^{-3} mmol (10.0 mg) of **4** were added to a round-bottom flask containing 50 mL of MB aqueous solution (10 mg L^{-1} or 0.03 mmol L^{-1}) and the system was stirred at room temperature under natural light. After 2, 5, 10, 12, 15 and 20 min, a 3-mL aliquot of the supernatant was taken to be analysed by UV-vis absorption spectroscopy. The absorbance peak at 664 nm, which corresponds to the n–π* transition of MB, was monitored. Alternatively, 1.0 mL of hydrogen peroxide (H_2O_2, 35%) was added to the MB solution under visible light before the addition of **4**. For the pH effect studies, the pH of the MB solutions was adjusted with diluted $HCl_{(aq)}$ or $NaOH_{(aq)}$ before the addition of **4**. The solids produced were isolated by centrifugation, washed three times with water and dried under vacuum. All reactions were performed at least in triplicate. The percentage of MB-bleaching was calculated according to the formula % = $(A_0 – A)/A_0 \times 100$, wherein A_0 = the initial absorbance of the MB solution and A = the absorbance at a given time point.

3. RESULTS AND DISCUSSION

3.1. Synthetic strategy

A vast array of synthetic routes has been employed for obtaining decavanadate compounds containing organic and inorganic counterions. Herein V_{10} salts containing trisH$^+$ have been synthesised using two different starting materials and methodologies (Scheme 1). The addition of an aqueous solution of tris to a solution of $NaVO_3$ produced a mixture of crystals containing $[trisH]_4[H_2V_{10}O_{28}]\cdot 10H_2O$ (**1**) and a fully inorganic sodium decavanadate salt, even after many attempts to adjust experimental conditions. On the other hand, the simple addition of an aqueous solution of tris to a V_2O_5 suspension slowly solubilised the oxide, producing an orange solution that gave pure orange crystals of $(trisH)_6[V_{10}O_{28}]$ (**2**) in good yield. While the normal solubility of V_2O_5 in water is 374 ppm, the tris aqueous solution was capable to solubilise 9080 ppm of the oxide and was twice as effective as the ionic liquid choline chloride-urea, a deep eutectic solvent [41].

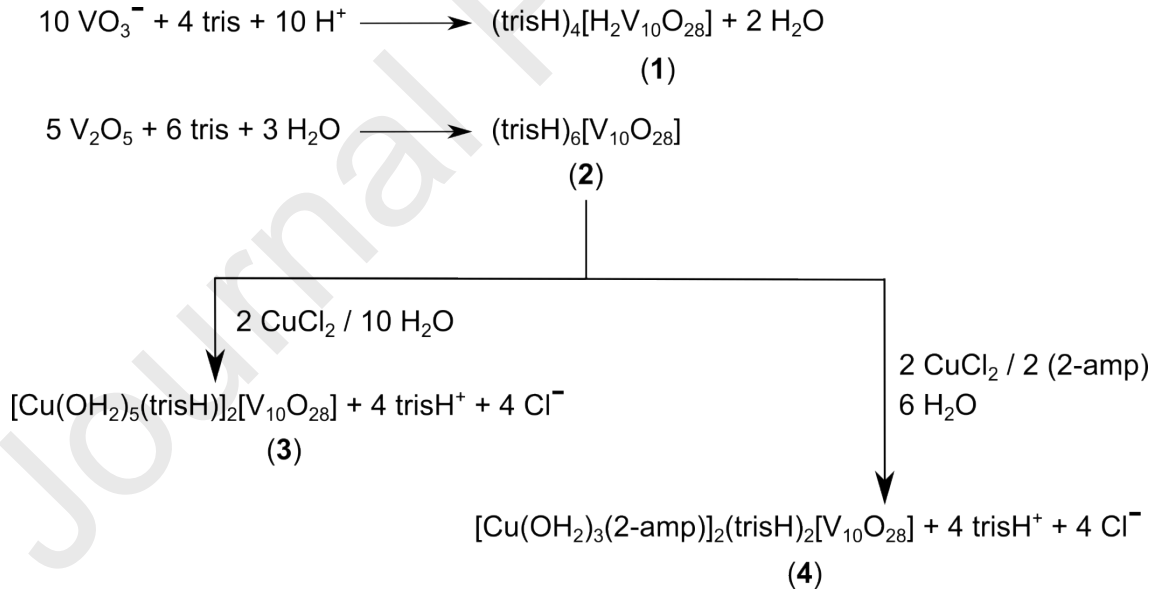

Scheme 1. Synthetic proposal for decavanadates with organic and copper(II) complex counterions from $NaVO_3$ and a V_2O_5 suspension in aqueous tris(hydroxymethyl)aminomethane.

During the synthesis of $(trisH)_6[V_{10}O_{28}]$ (**2**), the pH of the solution slowly decreased from 8 to 6 after 3 h, forming the V_{10} anion at room temperature in its fully deprotonated form (pKa of $[V_{10}O_{28}]^{6-}$ ranging from 5.5 to 6) [57, 58]. At pH = 6, tris is protonated to $trisH^+$ (pKa = 8.07 at 25 °C), favouring the formation of the salt over functionalised polyoxovanadates, as earlier reported for tetravanadates [33, 36], decavanadates [37] and, mainly, Lindqvist-type hexavanadates [33-35, 59]. Different from the route adopted here, these compounds have been usually synthesised under hydrothermal [28, 35, 37] and solvothermal [33, 34] conditions, or using inert atmosphere [29-32, 60] to obtain fully reduced [28, 29, 33, 37], fully oxidised [29-31], or mixed-valence [29, 33-36] polyoxovanadates (Table S1). In face of the previously reported interactions of vanadate with tris at room temperature [57], ^{51}V NMR analyses at pH 7.6 and 9.0 showed that, in such conditions, tris effectively coordinates to vanadium(V), giving a variety of vanadate esters with different geometries and V : tris ratios [57].

The extension of the route that produced **2** by the addition of a copper(II) salt gave $[Cu(OH_2)_5(trisH)]_2[V_{10}O_{28}]\cdot 6H_2O$ (**3**), under mild conditions and without additional purification steps. In face of this result, we decided to test if the same route would be useful to produce more complex structures. Aiming to carry out a sequential-one-pot preparation, the 2-amp pre-ligand was added to the reaction mixture, yielding $[Cu(OH_2)_3(2\text{–}amp)]_2(trisH)_2[V_{10}O_{28}]\cdot 2H_2O$ (**4**). The role played by tris seems to be similar to that played by ethylenediamine in the direct synthesis of a series of decavanadate derivatives containing copper(II)-ethylenediamine complexes [43], including $(H_2en)_2[Cu(en)_2(H_2O)_2][V_{10}O_{28}]$;

however, in that case, the reactions were performed under reflux and ammonium oxalate was added to the reaction medium.

3.2. Single-crystal X-ray diffraction analysis

Crystallographic data for products **1**-**4** are given in Table 1, and selected bond lengths and angles are shown in Tables 2 and 3. Since product **1** was not obtained pure, this work reports only its single-crystal X-ray diffraction structure, while products **2**-**4** were further characterized in the solid state. The structural moiety common to the complexes (**1**-**4**) is the decavanadate anion $[H_xV_{10}O_{28}]^{(6-x)-}$, with bond lengths and angles in the range found in the literature [16, 61]. V–O bond lengths vary between the four kinds of oxygen atoms in the following ranges: $V–O_{terminal}$ from 1.5919 to 1.6216 Å, $V–\mu_2$-O from 1.6763 to 2.0800 Å, $V–\mu_3$-O from 1.9175 to 2.0186 Å, and $V–\mu_6$-O from 2.0920 to 2.3430 Å. Longer V–O distances, in the order of 2.3 Å, are commonplace in vanadium oxide chemistry [62].

*3.2.1. Crystal structures of compounds **1** and **2***

The crystal structures of complexes $(trisH)_4[H_2V_{10}O_{28}]\cdot 10H_2O$ (**1**) and $(trisH)_6[V_{10}O_{28}]$ (**2**) are composed of V_{10} anions and organic $trisH^+$ cations. They differ from each other in the presence of water molecules in **1**, in the degree of protonation of the polyoxoanion and in the number of $trisH^+$ that balance its

charge, which was dictated by the pH of each reaction medium. The ORTEP diagrams and crystal packing of compounds **1** and **2** are presented in Figure 1.

Complex **1** crystallises in the P-1 triclinic space group and the asymmetric unit contains half an $[H_2V_{10}O_{28}]^{4-}$ anion, 2 $trisH^+$ cations and 5 water molecules. The V_{10} anion is caged in the unit cell and embedded by waters and $trisH^+$ cations in an extensive three-dimensional hydrogen bond network, with all the V_{10} anions aligned in each layer. A medium-strength hydrogen bond involving O(31)–H(31)···O(6) of a nearby $trisH^+$ cation (O…O donor-acceptor distance = 2.7096(19) Å, 175(6)°) defines a chain containing V_{10} and two $trisH^+$ along the *c* axis that also involves the medium-strength hydrogen bonds N(5)–H(2N5)···O(32) and O(8)–H(8)···O(28) (Figure S1), respectively. Along the *b* axis, the $trisH^+$ cation of N(1) interacts with V_{10} through hydrogen bonds between O3–H(3)···μ_3–O(26), and N(1)–H(2N1)···μ_2–O(29); it is also connected to three water molecules.

The structure of **1** contains cyclic water octamers, generated through O–H···O interactions and linked to the supramolecular structure by further rings formed by hydrogen bond interactions of the water molecule containing oxygen atom O(3W) with $trisH^+$ cations containing N(1) (Table S2). The appearance of water rings is not unknown in decavanadate supramolecular chemistry and they are especially present in highly hydrated structures [17, 63]. They can consist of cyclic structures formed only by water molecules [63] or by water molecules and counterions [17]. Recently, compounds $(DMAPH)_6[V_{10}O_{28}]\cdot H_2O$ and

$(DMAPH)_6[V_{10}O_{28}]\cdot 16H_2O$ (DMAPH = dimethylaminopyridinium) were isolated at 25 °C and 10 °C, respectively. In the latter, the water molecules form cyclic pentamers and hexamers involved in the stabilisation of the 3D network [63]. In $[4\text{-ampH}]_{10}[\{Na(H_2O)_6\}\{HV_{10}O_{28}\}][V_{10}O_{28}]\cdot 15H_2O$ [17], the sodium aquocomplex participates in a dumbbell-shaped cyclic water pentamer found in the supramolecular lattice of the compound.

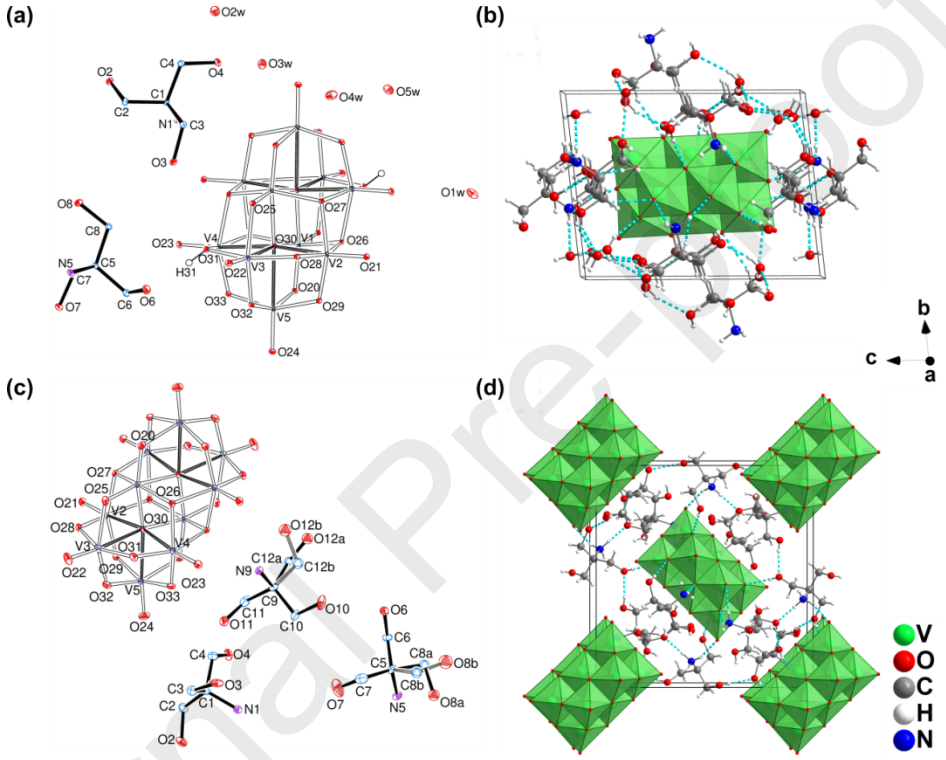

Figure 1. (a) and **(c)**: ORTEP representation with atom-labelling scheme of $(trisH)_4[H_2V_{10}O_{28}]\cdot 10H_2O$ (**1**) and $(trisH)_6[V_{10}O_{28}]$ (**2**), showing only the crystallographically independent water molecules and $trisH^+$ cations. Hydrogen atoms were omitted for clarity, except for those on the protonated decavanadate in **1**. Thermal ellipsoids were drawn at the 50% probability level. The dark bonds within the polyoxovanadate represent the longest V–O bonds found in the anion. **(b)** and **(d)**: Unit cell of (**1**) and (**2**), displaying Z = 1 and Z = 2, respectively.

The structure of **2** belongs to the monoclinic system, $P2_1/n$ space group, with the V_{10} anionic units lying across crystallographic inversion centres at the centre of the cell and at the cell vertices, giving a total of two $(trisH)_6[V_{10}O_{28}]$ (**2**) molecules per unit cell. The 3D crystal structure is stabilised by a complex hydrogen bond

network, which involves the fully deprotonated $[V_{10}O_{28}]^{6-}$ anions and $trisH^{+}$ cations; the organic cations are the sole electronic density donors of O–H···O, N–H···O and C–H···O interactions (Table S3). A view along the *a* axis demonstrates alternating layers of V_{10} anions oriented orthogonally to each other (Figure S2). Each V_{10} is connected to other V_{10} anions along the *a* axis through an extensive hydrogen bond network involving the $trisH^{+}$ cations containing N(9) and N(1). The N(5)-containing $trisH^{+}$, in turn, interacts strongly with other cations, but forms weaker hydrogen bonds with V_{10}.

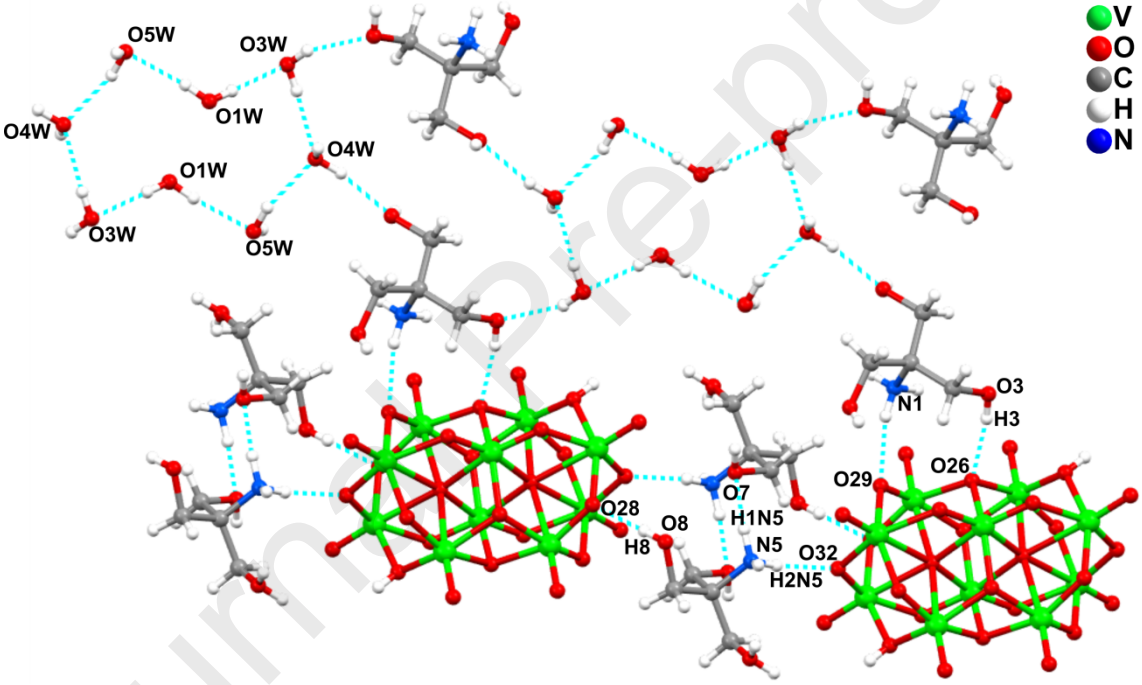

Figure 2. 2D sheet formed by O–H···O and N–H···O interactions of $trisH^{+}$ cations with V_{10} anions and water molecules in the lattice of $(trisH)_4[H_2V_{10}O_{28}]\cdot 10H_2O$ (**1**). In this view, the octamers formed by water molecules were evidenced.

As expected, the V(4)–O(31) bond length of 1.803(2) Å in the fully deprotonated V_{10} in **2** is shorter than the distance of 1.8723(12) Å observed for the equivalent bond in the protonated site of the $[H_2V_{10}O_{28}]^{4-}$ anion in **1**. Bond valence sums (BVS) [64], given by $\Sigma^S = \Sigma(d/1.791)^{-5.1}$ (d = V–O distances, S = bond number) for μ_3–O and μ_2–O bridging oxygens are given in Table S4. The low valence value

found for O(31), in the order of 1.5, remarkably lower than the valence values found for the remaining μ_3–O and μ_2–O atoms, confirms that O(31), along with the symmetrically related atom O(31^{i}), are the protonated sites. Thus, the protonation yielding the dihydrogendecavanadate anion in **1** occurred on doubly bridging oxygen atoms O(31) and O(31A), of intermediate basicity [16], and not on the most basic sites (the triply bridging oxygens).

In both crystalline structures of **1** and **2**, the V_{10} bridging oxygen atoms with the lowest BVS values generally participate in the strongest hydrogen bonds, as seen in Table S4. Hydrogen bonding distributes electronic density across the crystal lattice and helps balance the overall valence of atoms most deficient in electrons [65]. Atoms O(29), O(31) and O(33) in **2**, for instance, exhibit BVS values of 1.715, 1.714 and 1.651, respectively, and participate in hydrogen bonds whose angles are above 175°, characterising strong interactions.

*3.3.2. Single crystal structures of **3** and **4***

The X-ray diffraction analysis of $[Cu(OH_2)_5(trisH)]_2[V_{10}O_{28}]\cdot 6H_2O$ (**3**) showed one fully deprotonated $[V_{10}O_{28}]^{6-}$ anion along with two mononuclear copper(II) cation complexes and six lattice water molecules (Figure 3). Copper(II) in the $[(Cu(H_2O)_5(trisH)]^{3+}$ cation presents four water molecules occupying an equatorial plane, with an additional water molecule and one trisH^{+} ligand coordinated through hydroxyl oxygen O(2), completing the Jahn-Teller-distorted octahedron. Product **3** crystallises in the monoclinic centrosymmetric space group $P2_1/n$, with

the V_{10} ions localised on the inversion centre and on each vertex. The central V_{10} and the two cation complexes are positioned between two glide planes, while the other anions are orthogonally oriented and lie in parallel layers above and below these planes (Figure S3). Each V_{10} interacts with the cation complexes through hydrogen bonds involving terminal and bridging oxygens O(3W)–H(1W3)···O(33) (μ_2), O(4W)–H(2W4)···(O23) (terminal), N(1)–H(2N1)···O(28) ($-\mu_2$), O(2)–H(2)···O(27) (μ_3), forming a zig-zag structure along the *b* axis. The crystal structure is stabilised by a complex pattern of hydrogen bonds that also involves the three uncoordinated water molecules (Table S5).

Table 1. Crystallographic and refinement data for $(trisH)_4[H_2V_{10}O_{28}]\cdot 10H_2O$ (**1**), $(trisH)_6[V_{10}O_{28}]$ (**2**), $[Cu(OH_2)_5(trisH)]_2[V_{10}O_{28}]\cdot 6H_2O$ (**3**) and $[Cu(OH_2)_3(2\text{–}amp)]_2(trisH)_2[V_{10}O_{28}]\cdot 2H_2O$ (**4**)

	1	**2**	**3**	**4**
Elemental formula	$C_{16}H_{70}N_4O_{50}V_{10}$	$C_{24}H_{72}N_6O_{46}V_{10}$	$C_8H_{56}N_2O_{50}V_{10}Cu_2$	$C_{20}H_{56}N_6O_{42}V_{10}Cu_2$
Molar mass / g mol^{-1}	1628.16	1690.27	1617.02	1689.18
Crystal system, space group	Triclinic, *P*-1	Monoclinic, $P2_1/n$	Monoclinic, $P2_1/n$	Triclinic, *P*-1
a / Å	10.4309(7)	10.3934(6)	10.1240(3)	10.6095(5)
b / Å	11.0433(8)	16.3523(11)	14.1401(5)	10.8867(5)
c / Å	13.5205(10)	15.9974(10)	16.6837(6)	13.1588(7)
α / °	76.258(3)	90	90	67.971(2)
β / °	71.873(3)	91.132(2)	102.238(2)	70.075(2)
γ / °	65.063(2)	90	90	63.512(2)
Temperature / K	100(2)	300(2)	200(2)	299(2)
Volume / Å^3	1331.90(17)	2718.3(3)	2334.07(14)	1233.14(11)
Z	1	2	2	1
Density / mg m^{-3}	2.030	2.065	2.301	2.275
F(000)	824	1712	1612	842
Absorption coefficient / mm^{-1}	1.797	1.761	18.186	2.766
Crystal size / mm	0.393 x 0.259 x 0.124	0.152 x 0.125 x 0.106	0.232 x 0.149 x 0.092	0.195 x 0.130 x 0.047
θ range / °	3.0 to 27.5	3.2 to 27.0	4.7 to 79.0	3.0 to 27.5
Reflections collected	60077	128196	167920	61633
Unique data	6114 [R(int) = 0.040]	5923 [R(int) = 0.094]	5035 [R(int) = 0.073]	5642 [R(int) = 0.041]
Observed data, [I > 2σ(I)]	5285	4646	4391	4825
Number of parameters	457	510	437	486
Goodness of fit on F^2	1.058	1.033	1.066	1.066
R [I > 2σ(I)], R_w [I > 2σ(I)] (*)	R = 0.024, R_w = 0.058	R = 0.034, R_w = 0.074	R = 0.026, R_w = 0.058	R = 0.022, R_w = 0.053
R, R_w (all data) (*)	R = 0.032, R_w = 0.061	R = 0.054, R_w = 0.078	R = 0.034, R_w = 0.060	R = 0.031, R_w = 0.056
Largest diff. peak and hole / e Å^{-3}	0.70 and -0.35	1.72 and -0.53	0.43 and -0.56	0.33 and -0.57

$w = [\sigma^2(Fo^2)+(0.0268*P)^2+1.3691*P]^{-1}$ where $P = (Fo^2+2Fc^2)/3$ for **1**
$w = [\sigma^2(Fo^2)+(0.0324*P)^2+4.1605*P]^{-1}$ where $P = (Fo^2+2Fc^2)/3$ for **2**
$w = [\sigma^2(Fo^2)+(0.0291*P)^2+2.1662*P]^{-1}$ where $P = (Fo^2+2Fc^2)/3$ for **3**
$w = [\sigma^2(Fo^2)+(0.0254*P)^2+0.9221*P]^{-1}$ where $P = (Fo^2+2Fc^2)/3$ for **4**

Table 2. Selected bond lengths (Å) for $(trisH)_4[H_2V_{10}O_{28}]\cdot 10H_2O$ (**1**), $(trisH)_6[V_{10}O_{28}]$ (**2**), $[Cu(OH_2)_5(trisH)]_2[V_{10}O_{28}]\cdot 6H_2O$ (**3**) and $[Cu(OH_2)_3(2\text{–amp})]_2(trisH)_2[V_{10}O_{28}]\cdot 2H_2O$ (**4**), with estimated standard deviations in parentheses.

Bond lengths (Å)							
1		**2**		**3**		**4**	
V(1)–O(25)#1	1.6844(12)	V(1)–O(25)	1.6763(19)	V(1)–O(25)	1.6804(16)	V(1)–O(25)	1.6815(13)
V(1)–O(26)	1.9176(12)	V(1)–O(26)	1.9346(17)	V(1)–O(26)	1.9422(14)	V(1)–O(26)	1.9434(12)
V(3)–O(25)	2.0426(12)	V(3)–O(25)	2.080(2)	V(3)–O(25)	2.0439(16)	V(3)–O(25)#1	2.0467(14)
V(3)–O(30)	2.3429(12)	V(3)–O(30)	2.3209(18)	V(3)–O(30)#1	2.3397(15)	V(3)–O(30)	2.3289(12)
V(3)–O(32)	1.8307(12)	V(3)–O(32)	1.804(2)	V(3)–O(32)	1.8456(17)	V(3)–O(32)	1.8620(14)
V(4)–O(23)	1.6130(12)	V(4)–O(23)	1.6192(18)	V(4)–O(23)	1.6216(15)	V(4)–O(23)	1.6115(13)
V(4)–O(31)	1.8723(12)	V(4)–O(31)	1.803(2)	V(4)–O(31)	1.8192(16)	V(4)–O(31)	1.8315(14)
V(4)–O(26)#1	2.0142(12)	V(4)–O(26)	2.0010(18)	V(4)–O(26)	1.9980(15)	V(4)–O(26)#1	2.0079(13)
C(1)–N(1)	1.496(2)	C(1)–N(1)	1.493(4)	C(1)–N(1)	1.496(3)	C(1)–N(1)	1.491(3)
C(1)–C(2)	1.526(2)	C(1)–C(2)	1.527(4)	C(1)–C(2)	1.528(3)	C(1)–C(2)	1.534(3)
C(2)–O(2)	1.426(2)	C(2)–O(2)	1.414(4)	C(2)–O(2)	1.425(3)	C(2)–O(2)	1.412(3)
O(31)–H(31)	0.82(2)			Cu–O(2W)	2.4335(19)	Cu–N(6)	1.9825(19)
				Cu–O(4W)	1.9607(19)	Cu–O(2W)	2.2045(16)
						C(8)–N(13)	1.342(3)
						C(7)–C(8)	1.493(3)

Symmetry transformations used to generate equivalent atoms: #1 **–**x+1, **–**y+1, **–**z+1

Table 3. Selected angles (°) for $(trisH)_4[H_2V_{10}O_{28}]\cdot 10H_2O$ (**1**), $(trisH)_6[V_{10}O_{28}]$ (**2**), $[Cu(OH_2)_5(trisH)]_2[V_{10}O_{28}]\cdot 6H_2O$ (**3**) and $[Cu(OH_2)_3(2\text{-amp})]_2(trisH)_2[V_{10}O_{28}]\cdot 2H_2O$ (**4**), with estimated standard deviations in parentheses

Angles (°)							
1		**2**		**3**		**4**	
O(25)#1–V(1)–O(26)	97.81(5)	O(25)–V(1)–O(26)	98.64(8)	O(25)–V(1)–O(26)	97.05(7)	O(25)–V(1)–O(26)	96.71(6)
O(25)#1–V(1)–O(30)#1	87.70(5)	O(25)–V(1)–O(30)	88.34(8)	O(25)–V(1)–O(30)#1	87.94(7)	O(25)–V(1)–O(30)#1	87.59(6)
O(26)–V(1)–O(27)#1	155.73(5)	O(26)–V(1)–O(27)	155.34(8)	O(26)–V(1)–O(27)	155.41(6)	O(26)–V(1)–O(27)	155.44(5)
O(32)–V(3)–O(28)	91.45(5)	O(32)–V(3)–O(28)	92.15(8)	O(32)–V(3)–O(28)	90.73(7)	O(32)–V(3)–O(28)	90.17(6)
O(22)–V(3)–O(32)	103.23(6)	O(22)–V(3)–O(32)	104.42(11)	O(22)–V(3)–O(32)	103.07(8)	O(22)–V(3)–O(32)	102.82(7)
O(32)–V(3)–O(31)	91.28(5)	O(32)–V(3)–O(31)	91.99(9)	O(32)–V(3)–O(31)	91.15(7)	O(32)–V(3)–O(31)	91.67(6)
O(22)–V(3)–O(31)	101.27(6)	O(22)–V(3)–O(31)	100.42(10)	O(22)–V(3)–O(31)	101.47(8)	O(22)–V(3)–O(31)	103.53(7)
O(33)–V(4)–O(31)	95.01(6)	O(33)–V(4)–O(31)	95.87(9)	O(33)–V(4)–O(31)	95.29(7)	O(33)–V(4)–O(31)	94.37(6)
O(31)–V(4)–O(26)#1	87.98(5)	O(31)–V(4)–O(26)	90.50(8)	O(31)–V(4)–O(26)	89.27(7)	O(31)–V(4)–O(26)#1	89.23(6)
O(23)–V(4)–O(30)	174.67(5)	O(23)–V(4)–O(30)	174.29(9)	O(23)–V(4)–O(30)#1	175.80(7)	O(23)–V(4)–O(30)	174.26(6)
V(2)–O(27)–V(4)#1	101.00(5)	V(2)–O(27)–V(4)#1	100.77(8)	V(2)–O(27)–V(4)#1	100.41(6)	V(2)#1–O(27)–V(4)	100.24(6)
V(1)–O(30)–V(3)	170.02(6)	V(1)#1–O(30)–V(3)	169.52(9)	V(1)–O(30)–V(3)#1	171.06(8)	V(1)#1–O(30)–V(3)	86.97(4)
V(3)–O(32)–V(5)	114.58(6)	V(3)–O(32)–V(5)	114.69(10)	V(3)–O(32)–V(5)	114.28(8)	V(3)–O(32)–V(5)	112.87(7)
N(1)–C(1)–C(2)	108.97(14)	N(1)–C(1)–C(2)	108.8(2)	N(1)–C(1)–C(2)	107.25(19)	N(1)–C(1)–C(2)	106.53(16)
O(2)–C(2)–C(1)	110.51(14)	O(2)–C(2)–C(1)	109.9(2)	O(2)–C(2)–C(1)	111.7(2)	O(2)–C(2)–C(1)	109.91(17)
				O(3W)–Cu–O(1W)	86.51(8)	C(8)–N(13)–Cu	114.76(14)
				O(3W)–Cu–O(5W)	176.01(8)	N(6)–Cu–N(13)	82.68(8)
				O(1W)–Cu–O(5W)	92.56(9)	O(1W)–Cu–O(3W)	91.68(7)
				O(3W)–Cu–O(2W)	95.92(7)	N(13)–Cu–O(2W)	109.33(7)
				O(5W)–Cu–O(4W)	91.19(9)	N(13)–C(8)–C(7)	116.2(2)

Symmetry transformations used to generate equivalent atoms: #1 –x+1, –y+1, –z+1

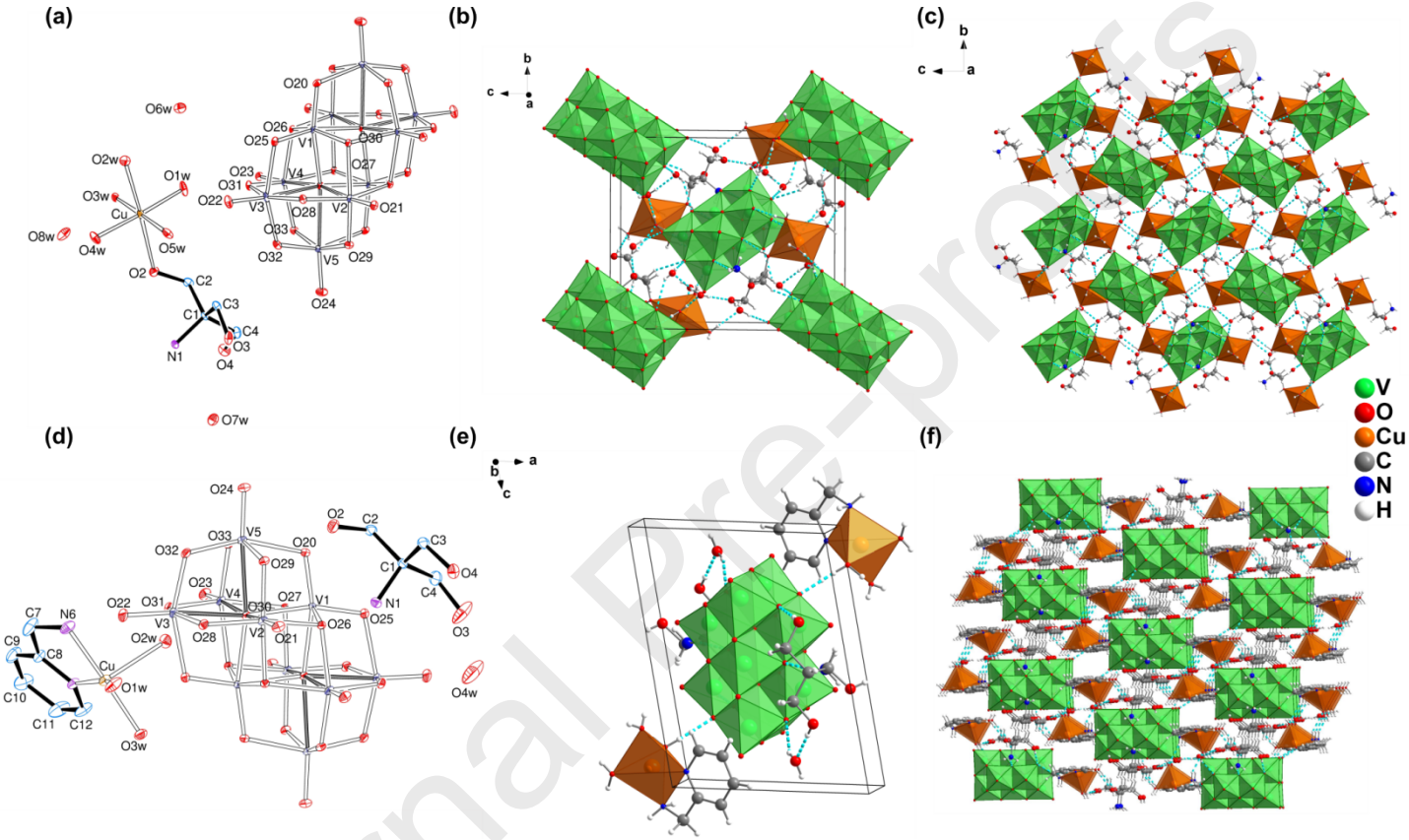

Figure 3. (a) and **(d)**: ORTEP representations of $[Cu(OH_2)_5(trisH)]_2[V_{10}O_{28}]\cdot 6H_2O$ (**3**) and $[Cu(OH_2)_3(2\text{–}amp)]_2(trisH)_2[V_{10}O_{28}]\cdot 2H_2O$ (**4**), showing only the crystallographically independent water molecules, $trisH^+$ cation and copper(II) complexes. Hydrogen atoms were omitted for clarity. Thermal ellipsoids were drawn at the 50% probability level. The dark bonds in decavanadate represent the longest V–O bonds found in the anion. **(b)** and **(e)**: Unit cell of complexes **3** and **4**, displaying Z = 2 and Z = 1, respectively. **(c)** and **(f)**: Expanded three-dimensional structures of complexes **3** and **4**. In **(f)** the layers are somewhat offset to evidence the presence of channels between two symmetry-related copper complexes. All chemical entities are connected by an intricate network of hydrogen bonds.

The structure of $[Cu(OH_2)_3(2–amp)]_2(trisH)_2[V_{10}O_{28}]\cdot 2H_2O$ (**4**) has been determined in the triclinic space group *P*-1, with Z = 1. Each V_{10} interacts electrostatically with two $trisH^+$ cations and two distorted square pyramidal copper(II) cations, $[Cu(OH_2)_3(2–amp)]^{2+}$; the copper centre is coordinated by one neutral, chelating bidentate 2–amp ligand and three water molecules which occupy the apical and two of the basal positions. Two water molecules fill the crystal packing of the structure (Figure 3) and are involved in an extensive hydrogen bond network with the ionic parts. Medium-strength interactions involve the hydroxyl groups of the $trisH^+$ cations, typically O(2)–H(2)···O(29) (O···O donor-acceptor distance = 2.718(2) Å, 174(3)°), and the aquo ligands of the copper(II) complexes, as O(2W)–H(1W2)···O(28) (O···O donor-acceptor distance = 2.657(2) Å, 172(3)°), with V_{10} as hydrogen bond acceptor in each case (Table S6). The strongest interaction in this compound happens between $trisH^+$ and the disordered lattice water molecule (O(3)–H(3)···O(4WA), (O(3)–H(3)···O(4WB)), presenting O···O donor-acceptor distances of 2.449(15) Å and 2.606(6) Å, and D–H···A donor-hydrogen-acceptor angles of 164(4)° and 163(3)°, respectively.

In the expanded crystal packing (Figure 3) in **4**, all decavanadates are aligned along the *c* axis. Pairs of square pyramidal $[Cu(OH_2)_3(2–amp)]_2^{2+}$ cation complexes (related by symmetry) are arranged around each of the cell vertices, and the bases of each pair are overlapping. Such a configuration gives rise to a 3D porous structure, defining cavities which present a 3.642-Å distance between the planes that contain two symmetry-related 2-amp aromatic rings (Figure S4).

A decavanadate compound, $[\{Cu(2–amp)_2(H_2O)\}_2H_2V_{10}O_{28}]\cdot 4H_2O$, with the copper(II) complex bound to V_{10} has been previously described [26]. This V_{10} derivative differs from **4** in that it is neutral, the copper(II) complex is hexacoordinated and presents two 2–amp ligands. The factors that determine the binding of the complex to V_{10} through a V_{10}–O–M bond or its arrangement as a counterion, balancing electrostatic forces, are not entirely understood yet. These structural variations may arise from the nature of the reactants and the stoichiometric proportions of 2–amp : Cu applied in each synthesis.

3.3. Vibrational spectroscopy

The infrared spectra of **2**, **3** and **4** (Figure S5, Table S7) present the expected decavanadate-related vibrations in the region below 1000 cm^{-1} [66]. The IR bands at 955 cm^{-1} (**2**) and 941 cm^{-1} (**3** and **4**) are assigned to ν(V=O). The bands in the range of 840 to *ca.* 600 cm^{-1} indicate the V–O–V stretching and angular deformation vibrations. The region above 3000 cm^{-1} presents a set of broad bands referent to ν(O–H) and ν(N–H) of tris and water molecules in the lattices. Further vibrations related to tris are observed in the region between 1600 and 1000 cm^{-1}, corresponding to δ(N–H), ν(C–C), δ(O–H), ν(C–N), and ν(C–O) [67]. The spectrum of **4** also presents a set of bands related to the pyridine ring of 2–amp between 1600 and 1000 cm^{-1} [68].

All products show characteristic bands of the tris counterion at the Raman spectra (Figure S6, Table S8), attributed to δ(N–H) at 1585 cm^{-1} (**2**), 1580 cm^{-1} (**3**) and 1572 cm^{-1} (**4**), as well as stretching and angular deformation of the carbon

skeleton around 1400 cm^{-1} and below 900 cm^{-1} [67]. The bands of V_{10} were observed at 984 cm^{-1} (**2**), 993 cm^{-1} (**3**) and 990 cm^{-1}, related to ν(V=O), and broad bands in the range of 970–760 cm^{-1}, ascribed to ν_{as}, ν_{s}, δ(V–O–V) [66]. Product **4** also presents weak bands attributed to $\nu(C–C)_{ring}$, β(CH), η(CH), and $\nu(C–N)_{ring}$ vibration modes of the 2–amp ligand in the range of 1570–1034 cm^{-1} [68].

3.4. Thermogravimetric analysis

The thermogram of **2** (Figure S7a) presented three mass loss steps observed at 206, 374 and 508 °C, corresponding to the thermal decomposition of the $trisH^+$ cations, to form CO_2, NO and H_2O [69]. The loss of 47.2% of the mass in different steps, instead of the expected thermal decomposition at *ca.* 300 °C [69], is a consequence of the extensive hydrogen bond net between the $trisH^+$ cations, between each cation with V_{10}, and of the molecular rearrangements that occur after the first mass losses. IR analysis of the solid treated above 600 °C corresponds to V_2O_5.

The thermograms of the bimetallic compounds are presented in Figures S7b and S7c. For **3**, the 21% mass loss observed up to 178 °C corresponds to the loss of 16 water molecules, six from the crystal lattice and ten coordinated in each $[(Cu(H_2O)_5(trisH)]^{3+}$ complex (Figure S7b). The last steps that go up to 430 °C are more complex and could correspond to the loss of the 2 $trisH^+$ followed by oxidation of the product to form more than one vanadium- and/or copper-based oxide. For **4**, the first two steps at 138 °C and 233 °C were attributed to the loss

of lattice and the copper(II)-complex water molecules (Figure S7c). The concomitant loss of the 2–amp ligands and the trisH$^+$ cations occurred from 233 to 472 °C due to the presence of strong hydrogen bonds involving trisH$^+$ and V_{10} (e.g. O(2)–H(2)...O(29), 176(4) °) and the chelating effect of the 2–amp ligand.

3.5. Solid state EPR studies for **3** and **4**

The X-band EPR spectra of pulverised samples of **3** and **4** at room temperature and 77 K are characteristic of mononuclear Cu^{II} species (Figure 4 and Figure S8). The absence of additional signals indicates that vanadium(V) was not reduced. The spectra of **3** showed three of the four expected hyperfine splitting lines of Cu^{II} (S = 1/2, *I* = 3/2) [70]. The simulated g-factor values (g_x = 2.0302, g_y = 2.1233 and g_z = 2.3923) obtained for **3** suggested a rhombic distortion from the octahedral geometry due to the combination of the coordination of tris and the dynamic Jahn-Teller effect [70, 71]. In this regard, XRD analysis of [Cu(H_2O)$_5$trisH]$^{3+}$ shows that the bond lengths in the *z* axis (average 2.514 Å) are longer than those observed in the *xy* plane, with Cu–O4W (1.9607(19) Å) slightly longer than the other Cu–OH_2 bonds (*ca* 1.940 Å). The rhombicity of the complex in the solid state can also be observed in the O–Cu–O angles of O(3W)–Cu–O(1W) (86.51(8)°), O(1W)–Cu–O(5W) (92.56(9)°) and O(3W)–Cu–O(2W) (95.92(7)°) and was also associated to the extensive hydrogen bond network that involves all ligands.

Simulated parameters for the spectrum of **4**, ($g_\perp$ (x,y) = 2.0711 and 2.0746 < $g_{||}$ (z) = 2.2466) reflect the axial symmetry of the g-tensor that originates from a

distorted square pyramid found in the $[Cu(OH_2)_3(2–amp)]^{2+}$ unit (τ = 0.33).[70] The absence of hyperfine splitting was associated with the electron density withdrawal by the 2–amp ligand's pyridine ring through the Cu–N bond [72].

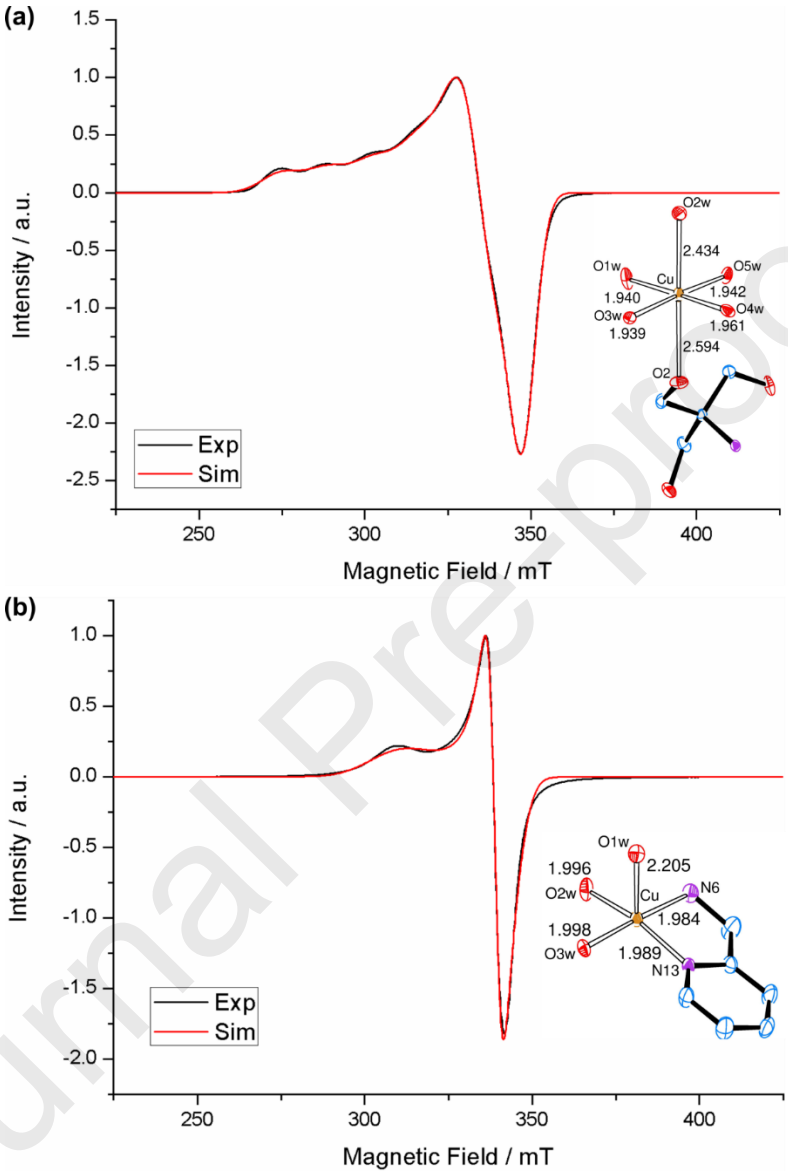

Figure 4. Experimental EPR spectra of products **3 (a)** and **4 (b)** in the solid state at room temperature: simulated (red line) and experimental (black line). For **3**: g_x = 2.0302, g_y = 2.1233 and g_z = 2.3923, $A_x = A_y$ < 50 MHz and A_z = 464.01 MHz. For **4**: $g_\perp$ (x,y) = 2.0711 and 2.0746 < $g_{||}$ (z) = 2.2466. Cationic complexes $[Cu(H_2O)_5trisH]^{3+}$ (top) and $[Cu(OH_2)_3(2–amp)]^{2+}$ (bottom) and their selected bond lengths are represented along each spectrum on the right.

3.6. Bleaching of methylene blue in aqueous solution

Since compounds **1**-**3** are highly soluble in water, only compound **4** was tested as a MB adsorbent, under stirring and at room temperature, in a variety of conditions. Firstly, the effect of the direct interaction of the polyoxovanadate with the dye solution was evaluated (Figure 5a). The absorbance at 664 nm, gradually decreased with time, achieving a solution bleaching of 84% after 20 min and giving a green-blue solid. No signal referent to vanadium(V) species was detected in the ^{51}V NMR spectrum of the supernatant, confirming that the vanadium(V) was not leached to the solution.

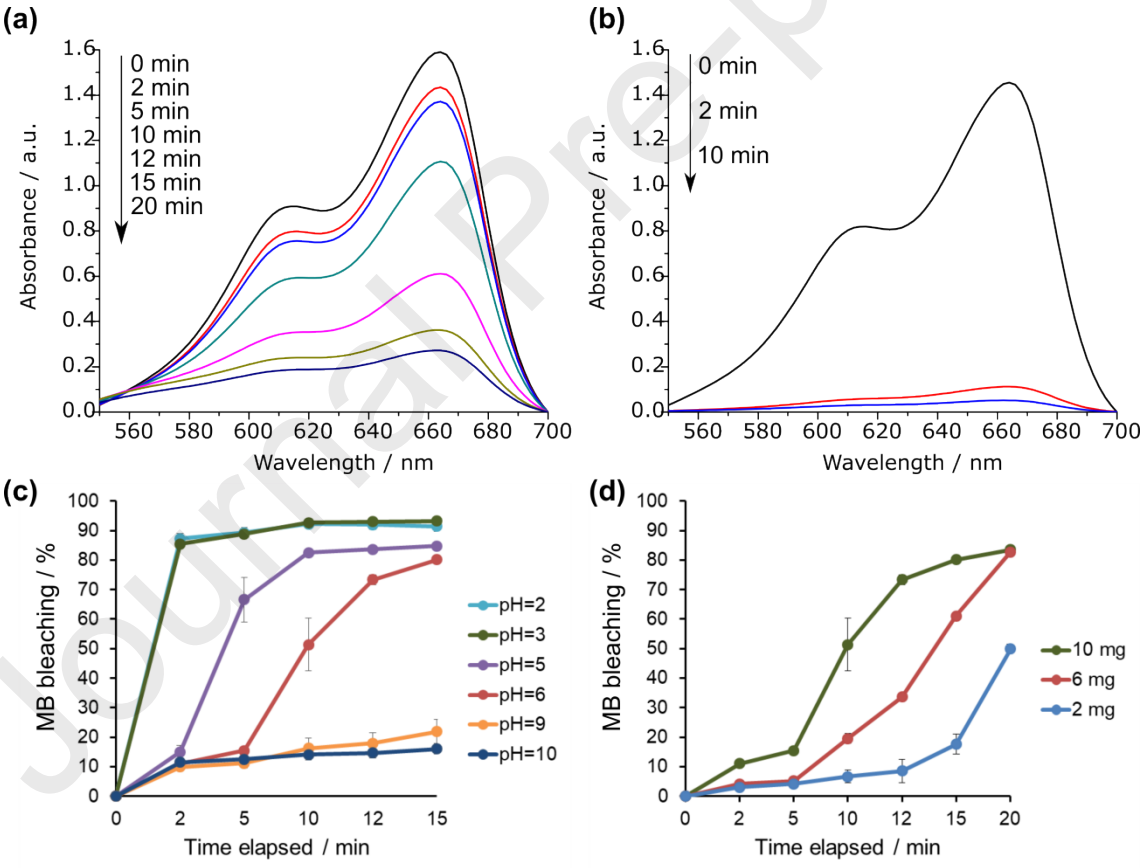

Figure 5. Absorption spectra of aqueous MB (0.03 mmol L^{-1}) in the range of 550 to 700 nm: **(a)** in the presence of **4** (10 mg) and **(b)** with the addition of H_2O_2 before the addition of **4**. Percentage of MB bleaching determined at 664 nm: **(c)** for the reactions with pH adjustment and **(d)** for the reactions with different amounts of **4**.

The addition of hydrogen peroxide, H_2O_2, improved the discolouration rate of MB by **4**, achieving 93% in 2 min (Figure 5b). This condition differs from the previous one in the presence of a low-intensity signal at –689 ppm in the ^{51}V NMR spectrum of the supernatant. This signal is characteristic of the mononuclear peroxovanadate $[H_2VO_2(O_2)_2]$ [73] (Figure S9), which could be related to the catalytic degradation of MB via an oxidative mechanism. Although this condition gave excellent bleaching of MB, *ca.* 5-7% desorption of MB was spectroscopically detected after 24 h, while in the reaction without H_2O_2 a permanent discolouration of the solution was observed for at least four months. Therefore, hereafter all the experiments were carried out without hydrogen peroxide.

The MB bleaching rate was pH-dependent, as shown in Figure 5c. The most acidic conditions reached discolouration of up to 90% after 2 min, producing a deep blue solid (**MB4-pH3**). This result is not entirely unexpected since the protonated form of MB interacts with the highly negative surface charge of the decavanadate anion [48, 74]. The reaction was smoother closer to environmental conditions (pH 5 and 6), presenting a decrease in the bleaching rate inasmuch as the pH increased, and giving a blue-green solid (**MB4-pH6**). Finally, the discolouration dropped considerably in basic media, achieving only 22% in pH 9, even after 15 min, accompanied by the disappearance of **4**. It is also well-known that decavanadate is stable in the pH range of 3 to 6, suffering hydrolysis under basic conditions, which might have contributed to the observed outcome [48].

Next, the adsorption performance was investigated varying the amount of **4** from 10 to 6 and 2 mg (Figure 5d) without pH adjustment. Although less effective, **4** was still able to remove 50% of MB from solution in 20 min at the lowest amount employed. Attempts to calculate the first and second order kinetic curves (data not shown) did not give any straight lines, suggesting that the bleaching might be a competition between more than one process, possibly both degradation and adsorption of the dye.

In order to gain some insight into the interaction of V_{10} with cationic dyes, a MB solution was slowly diffused into a sodium decavanadate aqueous solution (0.3 MB : 5 V) in preparative scale. After 24 h, green crystals of $(C_{16}H_{18}N_3S)_4[H_2V_{10}O_{28}]\cdot 15H_2O$ (**MBV$_{10}$**) were formed. Although these crystals were not suitable for single-crystal X-ray analysis, they were analysed by powder X-ray diffraction (Figure S10) and FTIR, and the latter was compared with those spectra from **MB4-pH3** and **MB4-pH6**. The FTIR spectrum of **MBV$_{10}$** showed bands that are compatible with MB and V_{10} (Figure 6). The spectral region from 1600 to 1000 cm^{-1} predominantly contains vibrations characteristic of MB, with ν(C=N) and ν(C–C) at 1599 and 1221 cm^{-1}, ν(C=S$^+$) at 1489 and 1356 cm^{-1}, δ(C–H) at 1441, 1392, 1252, and 1178 cm^{-1}, δ(C–N) at 1153 cm^{-1}, and ν(C–S–C) at 1040 cm^{-1} [75]. The region below 1000 cm^{-1} presented typical vibrations of the decavanadate anion at 964 cm^{-1} (ν(V=O)), 831, 760, and 607 cm^{-1} (ν_{as}, ν_s, δ (V–O–V), respectively) [66].

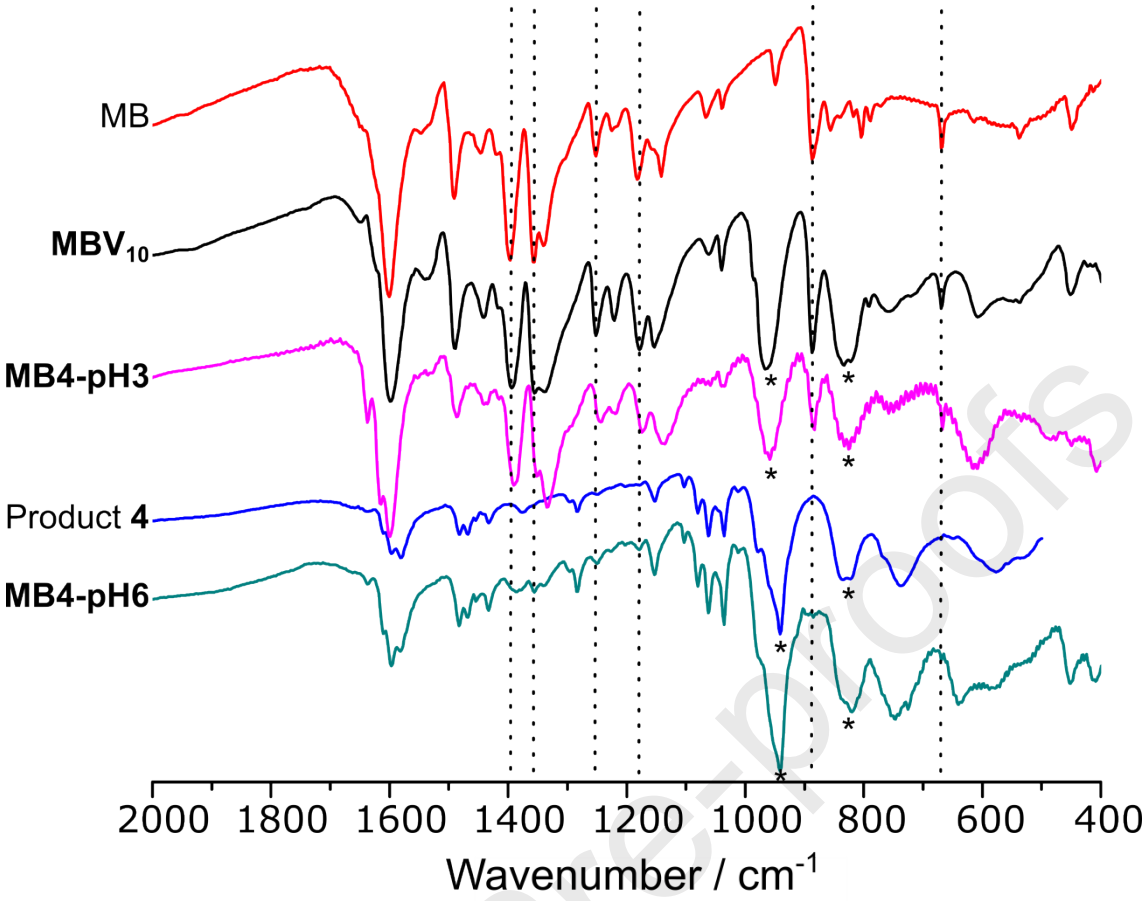

Figure 6. Comparative FTIR spectra of MB, **MBV_{10}**, **MB4-pH3**, product **4**, and **MB4-pH6**. The dotted vertical lines represent the MB bands common to the first three spectra. The asterisks (*) represent the decavanadate bands common to all spectra, except for MB.

The FTIR spectra of the solids isolated from different pH conditions were markedly distinct from each other (Figure 6). The spectrum of **MB4-pH3** is practically superimposable to that of **MBV_{10}**, which suggests that, at lower pH, the predominant process could be an exchange of the cation $[Cu(OH_2)_3(2–amp)]^{2+}$ for MB. This hypothesis is reinforced by the presence of a low-intensity signal with g = 2.083 in the EPR spectrum of the supernatant, probably related to the copper species that could have been released in solution. This kind of strategy was recently described by the adsorption of MB by $(NH_2Me_2)_{12}[(V_5O_9Cl)_6(1,4\text{-ndc})_{12}]$ (ndc = naftalene dicarboxylate) [76] and [2-

ampH]$_6$[$V_{10}O_{28}$]·2H_2O, wherein the high efficiency of the latter was explained by an exchange between 2-ampH cations for MB [48].

On the other hand, the absence of MB vibration modes in the spectrum of the solid at pH 6 (in three independent runs), strongly suggests that the structural integrity of compound **4** is maintained in conditions closer to neutrality and that MB was degraded. An expressive photocatalytic degradation of the dye under visible irradiation has also been reported for $V_{10}O_{16}(OH)_6(CH_3CH_2CO_2)_6]^{2-}$ [45], {[Ag(bpe)]$_4V_6O_{17}$}$_n$ (bpe = 1,2-di(4-pyridyl)ethylene,[77] and $[V_6(O)_{10}(pdc)_6]^{2-}$ (pdc = 2,6-pyridinedicarboxylate) [49], but the rate of the degradation were higher than the observed for **4**. At a first analysis, the bleaching pathway was dependent on the solution pH, which is intrinsically related to the solubility of **4**. Indeed, **4** was poorly soluble in slightly acidic to neutral water (pH 5 to 7), but its solubility increased at pH 3, favouring the interaction of V_{10} with MB precipitating.

4. CONCLUSIONS

Four new $V_{10}O_{28}$-based hybrid compounds have been synthesised, three of them *via* a simple pathway that employed tris to solubilise vanadium pentoxide under mild conditions. Advantages of the methodology are the use of non-hazardous chemical reactants and solvents, and the possibility to extend the route for the preparation of bimetallic systems, opening a path for the synthesis of V_{10} derivatives with other transition metals. The solid-state studies help bring light into the interactions of decavanadate with tris buffer and other related

compounds. Dramatic changes in the crystal packing were observed when the degree of hydration varies, giving rise to distinct associations between the constituents of the lattice. Compound $[Cu(OH_2)_3(2–amp)]_2(trisH)_2[V_{10}O_{28}]\cdot 2H_2O$ (**4**) was able to bleach an aqueous solution of MB in a pH-dependent form, by cation exchange in more acidic conditions. In less acidic conditions, the discolouration pathway is not clear yet, but, based on the results, it could be associated to a partial or complete degradation of the dye.

CONFLICTS OF INTEREST

There are no conflicts to declare.

APPENDIX A. SUPPLEMENTARY DATA

CCDC deposit numbers 1966465-1966468 contain the supplementary crystallographic data for $(trisH)_4[H_2V_{10}O_{28}]\cdot 10H_2O$ (**1**), $(trisH)_6[V_{10}O_{28}]$ (**2**), $[Cu(OH_2)_5(trisH)]_2[V_{10}O_{28}]\cdot 6H_2O$ (**3**) and $[Cu(OH_2)_3(2–amp)]_2(trisH)_2[V_{10}O_{28}]\cdot 2H_2O$ (**4**). These data can be obtained free of charge via http://www.ccdc.cam.ac.uk/conts/retrieving.html, or from the Cambridge Crystallographic Data Centre, 12 Union Road, Cambridge CB2 1EZ, UK; fax: (+44) 1223-336-033; or e-mail: deposit@ccdc.cam.ac.uk.

ACKNOWLEDGEMENTS

This work was financially supported by Coordenação de Aperfeiçoamento de Pessoal de Nível Superior (CAPES, PVE A099/2013), Financiadora de Estudos e Projetos (FINEP/CT-Infra). Authors thank Mr. Ângelo Roberto dos Santos Oliveira (UFPR) for the TGA analyses and LAMAQ, UTFPR for the metal analyses. The authors also thank Dr. Jaísa Fernandes Soares for the valuable discussions and helpful suggestions on this work. J.M.M., L.B.P.L., K.P., F.S.S., D.L.H., E.L.S., R.R.R., and G.G.N. thank CNPq, CAPES and the CAPES-PrInt program for research grants and scholarships.

REFERENCES

[1] Y. Hayashi, Hetero and lacunary polyoxovanadate chemistry: Synthesis, reactivity and structural aspects, Coordination Chemistry Reviews, 255 (2011) 2270-2280.
[2] U. Warzok, L.K. Mahnke, W. Bensch, Soluble hetero-polyoxovanadates and their solution chemistry analyzed by electrospray ionization mass spectrometry, Chemistry – A European Journal, 25 (2019) 1405-1419.
[3] B.E. Schurr, O. Nachtigall, L.E. VanGelder, J. Drappeau, W.W. Brennessel, E.M. Matson, Consequences of ligand derivatization on the electronic properties of polyoxovanadate-alkoxide clusters, Journal of Coordination Chemistry, 72 (2019) 1267-1286.
[4] M. Anjass, S. Greiner, M. Fichtner, C. Streb, Solid-state-stabilization of molecular vanadium oxides for reversible electrochemical charge storage, Inorganic Chemistry Frontiers, (2019) 134-139.
[5] K. Postal, D.F. Maluf, G. Valdameri, A.L. Rüdiger, D.L. Hughes, E.L. de Sá, R.R. Ribeiro, E.M. de Souza, J.F. Soares, G.G. Nunes, Chemoprotective activity of mixed valence polyoxovanadates against diethylsulphate in *E. coli* cultures: insights from solution speciation studies, RSC Advances, 6 (2016) 114955-114968.
[6] D. Marques-da-Silva, G. Fraqueza, R. Lagoa, A.A. Vannathan, S.S. Mal, M. Aureliano, Polyoxovanadate inhibition of *Escherichia coli* growth shows a reverse correlation with Ca^{2+}-ATPase inhibition, New Journal of Chemistry, 43 (2019) 17577-17587.

[7] J.-J. Chen, J.-C. Ye, X.-G. Zhang, M.D. Symes, S.-C. Fan, D.-L. Long, M.-S. Zheng, D.-Y. Wu, L. Cronin, Q.-F. Dong, Design and performance of rechargeable sodium ion batteries, and symmetrical Li-ion batteries with supercapacitor-like power density based upon polyoxovanadates, Advanced Energy Materials, 8 (2018) 1701021.
[8] W.-L. Li, E.-F. Ni, X.-H. Li, H.-J. Guo, Polyoxovanadate $(NH_4)_7[MnV_{13}O_{38}]$ as cathode material for lithium ion battery and improved electrochemical performance, Transactions of Nonferrous Metals Society of China, 26 (2016) 2372-2379.
[9] D. Gatteschi, L. Pardi, A.L. Barra, A. Müller, Polyoxovanadates: The missing link between simple paramagnets and bulk magnets?, Molecular Engineering, 3 (1993) 157-169.
[10] B. Tsukerblat, A. Tarantul, S. Aldoshin, A. Palii, Layered polyoxovanadate V_{15}: From structure to highly anisotropic magnetism, Journal of Coordination Chemistry, 71 (2018) 1-27.
[11] K. Wang, Q. Xu, P. Ma, C. Zhang, J. Wang, J. Niu, Polyoxovanadate catalysts for oxidation of 1-phenyl ethanol: from the discrete $[V_4O_{12}]^{4-}$ and $[V_{10}O_{28}]^{6-}$ anions to the anionic $[V_6O_{17}]_n^{4n-}$ coordination polymer, CrystEngComm, 20 (2018) 6273-6279.
[12] K. Wang, Y. Niu, D. Zhao, Y. Zhao, P. Ma, D. Zhang, J. Wang, J. Niu, The polyoxovanadate-based carboxylate derivative $K_6H[V^{(V)}_{17}V^{(IV)}_{12}(OH)_4O_{60}(OOC(CH_2)_4COO)_8].nH_2O$: Synthesis, crystal structure, and catalysis for oxidation of sulfides, Inorganic Chemistry, 56 (2017) 14053-14059.
[13] K. Kastner, M. Lechner, S. Weber, C. Streb, *In situ* assembly, de-metalation and induced repair of a copper-polyoxovanadate oxidation catalyst, ChemistrySelect, 2 (2017) 5542-5544.
[14] M. Aureliano, C.A. Ohlin, M.O. Vieira, M.P.M. Marques, W.H. Casey, L.A.E. Batista de Carvalho, Characterization of decavanadate and decaniobate solutions by Raman spectroscopy, Dalton Transactions, 45 (2016) 7391-7399.
[15] P.A. Winkler, Y. Huang, W. Sun, J. Du, W. Lü, Electron cryo-microscopy structure of a human TRPM4 channel, Nature, 552 (2017) 200.
[16] N. Bošnjaković-Pavlović, J. Prévost, A. Spasojević-de Biré, Crystallographic statistical study of decavanadate anion based-structures: Toward a prediction of noncovalent interactions, Crystal Growth & Design, 11 (2011) 3778-3789.
[17] S.R. Amanchi, S.K. Das, A versatile polyoxovanadate in diverse cation matrices: A supramolecular perspective, Frontiers in Chemistry, 6 (2018) 469.
[18] M.P. Franco, A.L. Rüdiger, J.F. Soares, G.G. Nunes, D.L. Hughes, Crystal structures of two deca-vanadates(V) with penta-aqua-manganese(II) pendant groups: $(NMe_4)_2[V_{10}O_{28}\{Mn(H_2O)_5\}_2]\cdot 5H_2O$ and $[NH_3C(CH_2OH)_3]_2[V_{10}O_{28}\{Mn(H_2O)_5\}_2]\cdot 2H_2O$, Acta Crystallographica Section E, 71 (2015) 146-150.
[19] S. Yerra, S.K. Das, Organic free decavanadate based materials: Inorganic linkers to obtain extended structures, Journal of Molecular Structure, 1146 (2017) 23-31.
[20] T. Higami, M. Hashimoto, S. Okeya, $[Ni(H_2O)_6]_2[Na(H_2O)_3]_2[V_{10}O_{28}].4H_2O$, bis(nickel hexahydrate) bis(sodium trihydrate) decavanadate tetrahydrate, Acta Crystallographica Section C, 58 (2002) i144-i146.
[21] J. Martin-Caballero, A. San Jose Wery, S. Reinoso, B. Artetxe, L. San Felices, B. El Bakkali, G. Trautwein, J. Alcaniz-Monge, J.L. Vilas, J.M. Gutierrez-

Zorrilla, A robust open framework formed by decavanadate clusters and copper(II) complexes of macrocyclic polyamines: Permanent microporosity and catalytic oxidation of cycloalkanes, Inorganic Chemistry, 55 (2016) 4970-4979.
[22] D. Venegas-Yazigi, P. Hermosilla-Ibáñez, J. Costamagna, E. Spodine, A. Vega, V. Paredes-García, E. Le Fur, A novel coordination polymer based on decavanadate units linked by copper(II) ethylenediamine complexes, Macromolecular Symposia, 304 (2011) 80-86.
[23] L. Klištincová, E. Rakovský, P. Schwendt, Decavanadate ion as bridging ligand. Synthesis and crystal structure of $(NH_4)_2[Cu_2(NH_3CH_2CH_2COO)_4(V_{10}O_{28})]\cdot 10H_2O$, Inorganic Chemistry Communications, 11 (2008) 1140-1142.
[24] A.K. Iyer, S. Roy, R. Haridasan, S. Sarkar, S.C. Peter, Ligand mediated valence fluctuation of copper in new hybrid materials constructed from decavanadate and a Cu(1,10-phenanthroline) complex, Dalton Transactions, 43 (2014) 2153-2160.
[25] Q.-H. Zhao, L. Du, R.-B. Fang, Bis(trimethylenediammonium) hexaaquacopper(II) decavanadate heptahydrate, Acta Crystallographica Section E, 62 (2006) m360-m362.
[26] L. Bartošová, Z. Padělková, E. Rakovský, P. Schwendt, Synthesis and crystal structure of two copper(II) complexes with coordinated decavanadate ion, Polyhedron, 31 (2012) 565-569.
[27] B. Huang, Z. Xiao, Y. Wang, D. Ke, C. Zhu, S. Zhang, X. Hu, P. Wu, Destroy the inherent symmetry of vanadium-based inorganic cluster through chiral organic ligand: Synthesis and characterization of a polyoxovanadate-derived amino acid ester hybrid, Journal of Molecular Structure, 1195 (2019) 10-16.
[28] Y. Xie, B. Huang, C. Xu, X. Hu, W. Chen, Z. Xiao, P. Wu, A novel 3D network constructed from tetra-substituted trisalkoxy-hexavanadate clusters: $Na_2[V^{IV}_6O_7\{(OCH_2)_3CNH_2\}_4]$, Inorganic Chemistry Communications, 84 (2017) 96-98.
[29] Q. Chen, D.P. Goshorn, C.P. Scholes, X.L. Tan, J. Zubieta, Coordination compounds of polyoxovanadates with a hexametalate core. Chemical and structural characterization of $[V^V_6O_{13}[(OCH_2)_3CR]_2]^{2-}$, $[V^V_6O_{11}(OH)_2[(OCH_2)_3CR]_2]$, $[V^{IV}_4V^V_2O_9(OH)_4[(OCH_2)_3CR]_2]^{2-}$, and $[V^{IV}_6O_7(OH)_6](OCH_2)_3CR]_2]_2$, Journal of the American Chemical Society, 114 (1992) 4667-4681.
[30] C. Allain, S. Favette, L.-M. Chamoreau, J. Vaissermann, L. Ruhlmann, B. Hasenknopf, Hybrid organic–inorganic porphyrin–polyoxometalate complexes, European Journal of Inorganic Chemistry, 2008 (2008) 3433-3441.
[31] W. Ju, X. Song, G. Yan, K. Xu, J. Wang, D. Yin, L. Li, X. Qu, Y. Li, J. Li, Layer-by-layer assembly of polyoxometalate–pyrene-decorated fluorescent microspheres for the suspension immunoassay of *Listeria monocytogenes*, Journal of Materials Chemistry B, 4 (2016) 4287-4294.
[32] D. Li, J. Song, P. Yin, S. Simotwo, A.J. Bassler, Y. Aung, J.E. Roberts, K.I. Hardcastle, C.L. Hill, T. Liu, Inorganic–organic hybrid vesicles with counterion- and pH-controlled fluorescent properties, Journal of the American Chemical Society, 133 (2011) 14010-14016.
[33] O. Nachtigall, A. Hagenbach, J. Wiecko, D. Lentz, U. Abram, J. Spandl, Functional polyoxometalates from solvothermal reactions of $VOSO_4$ with tripodal alkoxides – a study on the reactivity of different “tris” derivatives, Dalton Transactions, 46 (2017) 509-516.

[34] O. Nachtigall, J. Spandl, Versatile organic chemistry on vanadium-based multi-electron reservoirs, Chemistry – A European Journal, 24 (2018) 2785-2789.
[35] Y. Wei, Z. Xiao, X. Hu, X. Hu, B. Huang, M. Cheng, P. Wu, X. Lin, Syntheses and post-functionalization of tri-substituted polyalkoxohexavanadates containing tris(alkoxo) ligands, Dalton Transactions, 46 (2017) 8505-8513.
[36] P. Zabierowski, M. Radoń, J. Szklarzewicz, W. Nitek, Mixed-valence V^{IV}/V^{V} tetrametallate core $\{V_4N_2O_{14}\}$ cluster containing tris(hydroxymethyl)aminomethane and acetylacetone, Inorganic Chemistry Communications, 41 (2014) 72-75.
[37] M.I. Khan, Q. Chen, D.P. Goshorn, H. Hope, S. Parkin, J. Zubieta, Polyoxo alkoxides of vanadium: the structures of the decanuclear vanadium(IV) clusters $[V_{10}O_{16}\{CH_3CH_2C(CH_2O)_3\}_4]^{4-}$ and $[V_{10}O_{13}\{CH_3CH_2C(CH_2O)_3\}_5]$, Journal of the American Chemical Society, 114 (1992) 3341-3346.
[38] A. Bayaguud, J. Zhang, R.N. Khan, J. Hao, Y. Wei, A redox active triad nanorod constructed from covalently interlinked organo-hexametalates, Chemical Communications, 50 (2014) 13150-13152.
[39] J.W. Han, C.L. Hill, A coordination network that catalyzes O_2-based oxidations, Journal of the American Chemical Society, 129 (2007) 15094-15095.
[40] B. Dong, Y. Chen, J. Peng, Y. Kong, Z. Han, Hydrothermal synthesis and crystal structure of a new mixed-valence mesostructured hexadecavanadate, Journal of Molecular Structure, 748 (2005) 171-176.
[41] P. Billik, P. Antal, R. Gyepes, Product of dissolution of V_2O_5 in the choline chloride–urea deep eutectic solvent, Inorganic Chemistry Communications, 60 (2015) 37-40.
[42] J.M. Missina, B. Gavinho, K. Postal, F.S. Santana, G. Valdameri, E.M. de Souza, D.L. Hughes, M.I. Ramirez, J.F. Soares, G.G. Nunes, Effects of decavanadate salts with organic and inorganic cations on *Escherichia coli*, *Giardia intestinalis*, and Vero cells, Inorganic Chemistry, 57 (2018) 11930-11941.
[43] M.V. Pavliuk, V.G. Makhankova, O.V. Khavryuchenko, V.N. Kokozay, I.V. Omelchenko, O.V. Shishkin, J. Jezierska, Decavanadates decorated with $[Cu(en)_2]^{2+}$: Convenient synthetic route, crystal structures and analysis of vibrational spectra, Polyhedron, 81 (2014) 597-606.
[44] S. Balu, K. Uma, G.-T. Pan, T.C.K. Yang, S.K. Ramaraj, Degradation of methylene blue dye in the presence of visible light using SiO_2@α-Fe_2O_3 nanocomposites deposited on SnS_2 flowers, Materials, 11 (2018) 1030.
[45] K. Wang, Y. He, Y. Zhao, P. Ma, J. Wang, A propionate-functionalized polyoxovanadate $K_2[V_{10}O_{16}(OH)_6(CH_3CH_2CO_2)_6]\cdot 20H_2O$: As catalyst for degradation of methylene blue, Journal of Molecular Structure, 1195 (2019) 184-188.
[46] J.-H. Yu, S.-H. Nam, J.W. Lee, D.I. Kim, J.-H. Boo, Oxidation state and structural studies of vanadium-doped titania particles for the visible light-driven photocatalytic activity, Applied Surface Science, 472 (2019) 46-53.
[47] S. Liang, Y.-M. Nie, S.-H. Li, J.-L. Zhou, J. Yan, A comprehensive study on the dye adsorption behavior of polyoxometalate-complex nano-hybrids containing classic β-octamolybdate and biimidazole units, Molecules, 24 (2019) 806.
[48] H. Naslhajian, M. Amini, S.M.F. Farnia, A. Sheykhi, O. Şahin, O.Z. Yeşilel, A new decavanadate polyoxovanadate nanocluster: synthesis, characterization and rapid adsorption of methylene blue, Journal of Coordination Chemistry, 70 (2017) 2940-2949.

[49] R.J. Batrice, J.N. Wacker, E.N. Glass, S.Z. Jilani, Y.J. Tong, M. Nyman, K.E. Knope, Template-free cyclic hexavanadate: Synthesis, characterization, solid-state structure, and solution-state dynamics, Polyhedron, 169 (2019) 266-277.
[50] S. Stoll, A. Schweiger, EasySpin, a comprehensive software package for spectral simulation and analysis in EPR, Journal of magnetic resonance (San Diego, Calif. : 1997), 178 (2006) 42-55.
[51] Program APEX2, in, Bruker AXS Inc., Madison, WI, 2010.
[52] Program APEX3, in, Bruker AXS Inc., Madison, WI, 2015.
[53] G. Sheldrick, SHELXT - Integrated space-group and crystal-structure determination, Acta Crystallographica Section A, 71 (2015) 3-8.
[54] International tables for X-ray crystallography, Kluwer Academic Publishers, Dordrecht, C (1992) 193, 219 and 500.
[55] L. Farrugia, WinGX and ORTEP for Windows: an update, Journal of Applied Crystallography, 45 (2012) 849-854.
[56] D.H.P.D.K.B. GbR, Diamond - Crystal and Molecular Structure Visualization, in, Crystal Impact, Kreuzherrenstr. 102, 53227 Bonn, Germany.
[57] A.S. Tracey, M.J. Gresser, Vanadium(V) oxyanions: interactions of vanadate with 1,1,1-tris(hydroxymethyl)ethane and with the buffer tris(hydroxymethyl)aminomethane, Inorganic Chemistry, 27 (1988) 1269-1275.
[58] D.C. Crans, B.J. Peters, X. Wu, C.C. McLauchlan, Does anion-cation organization in Na^+-containing X-ray crystal structures relate to solution interactions in inhomogeneous nanoscale environments: Sodium-decavanadate in solid state materials, minerals, and microemulsions, Coordination Chemistry Reviews, 344 (2017) 115-130.
[59] Z. Xiao, K. Chen, B. Wu, W. Li, P. Wu, Y. Wei, An easy way to construct polyoxovanadate-based organic–inorganic hybrids by stepwise functionalization, European Journal of Inorganic Chemistry, 2016 (2016) 808-811.
[60] C.P. Pradeep, D.-L. Long, G.N. Newton, Y.-F. Song, L. Cronin, Supramolecular metal oxides: Programmed hierarchical assembly of a protein-sized 21 kDa $[(C_{16}H_{36}N)_{19}\{H_2NC(CH_2O)_3P_2V_3W_{15}O_{59}\}_4]^{5-}$ polyoxometalate assembly, Angewandte Chemie International Edition, 47 (2008) 4388-4391.
[61] H.T. Evans, The molecular structure of the isopoly complex ion, decavanadate ($V_{10}O_{28}^{6-}$), Inorganic Chemistry, 5 (1966) 967-977.
[62] F.D. Hardcastle, I.E. Wachs, Determination of vanadium-oxygen bond distances and bond orders by Raman spectroscopy, The Journal of Physical Chemistry, 95 (1991) 5031-5041.
[63] E. Sánchez-Lara, A. Pérez-Benítez, S. Treviño, A. Mendoza, F.J. Meléndez, E. Sánchez-Mora, S. Bernès, E. González-Vergara, Synthesis and 3D network architecture of 1- and 16-hydrated salts of 4-dimethylaminopyridinium decavanadate, $(DMAPH)_6[V_{10}O_{28}]\cdot nH_2O$, Crystals, 6 (2016) 65.
[64] W.G. Klemperer, W. Shum, Charge distribution in large polyoxoanions: determination of protonation sites in vanadate ($V_{10}O_{28}^{6-}$)by oxygen-17 nuclear magnetic resonance, Journal of the American Chemical Society, 99 (1977) 3544-3545.
[65] F.C. Hawthorne, The role of OH and H_2O in oxide and oxysalt minerals, Zeitschrift für Kristallographie - Crystalline Materials, 1992, pp. 183.
[66] R.L. Frost, K.L. Erickson, M.L. Weier, O. Carmody, Raman and infrared spectroscopy of selected vanadates, Spectrochimica Acta. Part A, Molecular and Biomolecular Spectroscopy, 61 (2005) 829-834.

[67] S. Schroetter-Dirks, D. Bougeard, Vibrational spectra of tris(hydroxymethyl)aminomethane hydrogenhalides $TRISH^{+}X^{-}$, $(HOH_2C)_3C–NH_3^{+}\cdot X^{-}$ (X=F, Cl, Br, I), Journal of Molecular Structure, 661-662 (2003) 109-119.
[68] S.P. Jose, S. Mohan, Vibrational spectra and normal co-ordinate analysis of 2-aminopyridine and 2-amino picoline, Spectrochimica Acta. Part A, Molecular and Biomolecular Spectroscopy, 64 (2006) 240-245.
[69] L.P. Bauermann, J. Bill, F. Aldinger, Bio-friendly synthesis of ZnO nanoparticles in aqueous solution at near-neutral pH and low temperature, The Journal of Physical Chemistry B, 110 (2006) 5182-5185.
[70] B.J. Hathaway, D.E. Billing, The electronic properties and stereochemistry of mono-nuclear complexes of the copper(II) ion, Coordination Chemistry Reviews, 5 (1970) 143-207.
[71] M.A. Hitchman, C.J. Simmons, H. Stratemeier, EPR of two Cu^{2+} complexes showing dynamic Jahn-Teller effects, Applied Magnetic Resonance, 19 (2000) 121-131.
[72] E. Carter, K.M. Sharples, J.A. Platts, D.M. Murphy, Structure determination of bound nitrogen-based adducts with copper(II) acetylacetonato; an EPR, ENDOR and DFT study, Physical Chemistry Chemical Physics, 17 (2015) 11445-11454.
[73] O.W. Howarth, Vanadium-51 NMR, Progress in Nuclear Magnetic Resonance Spectroscopy, 22 (1990) 453-485.
[74] M. Findik, A. Ucar, A. Tolga Colak, O. Sahin, H. Bingol, U. Sayin, N. Kocak, Self-assembly of a new building block of $\{BMo_{12}O_{40}\}$ with excellent catalytic activity for methylene blue, Polyhedron, 160 (2019) 229-237.
[75] O.V. Ovchinnikov, A.V. Evtukhova, T.S. Kondratenko, M.S. Smirnov, V.Y. Khokhlov, O.V. Erina, Manifestation of intermolecular interactions in FTIR spectra of methylene blue molecules, Vibrational Spectroscopy, 86 (2016) 181-189.
[76] Y. Tao, N. Xu, X. Wang, Z. Su, Polyoxovanadate-based metal−organic octahedron based on 1,4-naphthalenedicarboxylic acid, Israel Journal of Chemistry, 59 (2019) 306-310.
[77] X. Xin, X. Tian, H. Zhang, Y. Gao, Y. Ma, Z. Han, Synthesis and characterization of Ag-ligand modified polyoxovanadates with three-dimensional structures, Journal of Solid State Chemistry, 269 (2019) 278-284.